RESEARCH ARTICLE

Innexin7a forms junctions that stabilize the basal membrane during cellularization of the blastoderm in *Tribolium castaneum*

Maurijn van der Zee[1,2,‡], Matthew A. Benton[3,*], Tania Vazquez-Faci[2], Gerda E. M. Lamers[2], Chris G. C. Jacobs[2] and Catherine Rabouille[1,4]

ABSTRACT

In insects, the fertilized egg undergoes a series of rapid nuclear divisions before the syncytial blastoderm starts to cellularize. Cellularization has been extensively studied in *Drosophila melanogaster*, but its thick columnar blastoderm is unusual among insects. We therefore set out to describe cellularization in the beetle *Tribolium castaneum*, the embryos of which exhibit a thin blastoderm of cuboidal cells, like most insects. Using immunohistochemistry, live imaging and transmission electron microscopy, we describe several striking differences to cellularization in *Drosophila*, including the formation of junctions between the forming basal membrane and the yolk plasmalemma. To identify the nature of this novel junction, we used the parental RNAi technique for a small-scale screen of junction proteins. We find that maternal knockdown of *Tribolium innexin7a* (*Tc-inx7a*), an ortholog of the *Drosophila* gap junction gene *Innexin 7*, leads to failure of cellularization. In Inx7a-depleted eggs, the invaginated plasma membrane retracts when basal cell closure normally begins. Furthermore, transiently expressed tagged Inx7a localizes to the nascent basal membrane of the forming cells in wild-type eggs. We propose that Inx7a forms the newly identified junctions that stabilize the forming basal membrane and enable basal cell closure. We put forward *Tribolium* as a model for studying a more ancestral mode of cellularization in insects.

KEY WORDS: Flour beetle, Armadillo, Actin, Time-lapse movie, Parental RNAi, Transient protein expression

INTRODUCTION

In most insects, the nuclei of the fertilized egg divide multiple times and move to the cortex before cellularization starts. During cellularization, plasma membrane ingresses between the nuclei and encloses them within individual cells (reviewed by Harris et al., 2009; Lecuit, 2004; Mazumdar and Mazumdar, 2002). In *Drosophila*, cellularization comprises different phases: a preliminary phase of membrane ingression, during which the so-called furrow canals are established (see below); a phase of slow membrane extension accompanied by elongation of the nuclei; a rapid phase of membrane extension required for the formation of tall columnar epidermal cells; and, finally, basal closure of the cells by means of actin rings (Schejter and Wieschaus, 1993). The cells that are formed are tall and narrow.

The formation of the furrow canals during the preliminary phase is a conspicuous start to cellularization in *Drosophila*. The furrow canals are the dilated leading edges of the ingressing membrane to which actin is recruited so that an apical interconnected hexagonal actin network is formed around each nucleus (Warn and Magrath, 1983). This network ingresses during membrane extension. The furrow canals are separated from the rest of the ingressing membrane by basal adherens junctions (BAJs). Main components of the BAJs are β-catenin (Armadillo) and E-cadherin (DEcad, or Shotgun) (reviewed by Lecuit, 2004).

Polarized membrane insertion appears to be the main force driving membrane extension (Lecuit and Wieschaus, 2000). Genes required for cellularization include key regulators of membrane trafficking, such as *Rab11* and *nuf* (Pelissier et al., 2003; Riggs et al., 2003; Rothwell et al., 1998) and zygotic genes such as *slam* (Acharya et al., 2014) and *nullo*. The latter is involved in the regulation of F-actin at the furrow canals, which is required for stabilization of the cleavage furrow (Sokac and Wieschaus, 2008a,b). In *nullo* mutants, some furrows regress during the phase of membrane extension (Sokac and Wieschaus, 2008b).

Whereas cellularization is well studied in *Drosophila*, it is unclear to what extent the molecular mechanisms underlying cellularization are conserved in other insects. *Tribolium castaneum* is a beetle that exhibits traits more ancestral for insects than *Drosophila*, such as short germ development (Schröder et al., 2008). Also, the thin blastoderm of cuboidal cells seen in *Tribolium* is more typical for insects than the columnar cells of the *Drosophila* blastoderm (Handel et al., 2000). Hence, we set out to describe cellularization in this beetle using live imaging techniques with transient expression of the membrane marker GAP43-YFP and the filamentous actin marker LifeAct-GFP (Benton et al., 2013), immunohistochemistry and transmission electron microscopy (TEM). We describe several key differences to *Drosophila* cellularization, the principal being the formation of junctions along the forming basal membrane.

To identify the nature of these junctions, we performed a small-scale parental RNAi (pRNAi) screen targeting junction proteins, and found that Innexin7a (Inx7a), a *Tribolium* ortholog of the *Drosophila* gap junction protein Innexin 7, has an essential role in cellularization. Innexin 7 function has been studied and appears to have no role in cellularization in *Drosophila* (Bauer et al., 2005; Ostrowski et al., 2008; Phelan, 2005). Innexins are a family of proteins related to the vertebrate Pannexins (Abascal and Zardoya, 2013; Baranova et al., 2004; Fushiki et al., 2010; Panchina et al., 2000) and functionally similar to the vertebrate Connexins (Alexopoulos et al., 2004; D'hondt et al., 2009; Goodenough and Paul, 2009; Meşe et al., 2007; Scemes et al., 2007). Innexins contain four transmembrane (TM) domains, two extracellular loops and intracellular N- and C-termini. Groups of six protein units assemble into homomeric or heteromeric hemichannels. Interaction *in trans* of two hemichannels in adjacent membranes is mediated by the

[1]Hubrecht Institute for Developmental Biology and Stem Cell Research, Uppsalalaan 8, Utrecht 3584 CT, The Netherlands. [2]Institute of Biology, Leiden University, Sylviusweg 72, Leiden 2333 BE, The Netherlands. [3]Department of Zoology, University of Cambridge, Downing Street, Cambridge CB2 3EJ, UK. [4]Department of Cell Biology, UMC Utrecht, 3584 CX Utrecht, The Netherlands. *Present address: Institute for Developmental Biology, University of Cologne, Zülpicherstrasse 47b, Cologne 50674, Germany.

‡Author for correspondence (m.van.der.zee@biology.leidenuniv.nl)
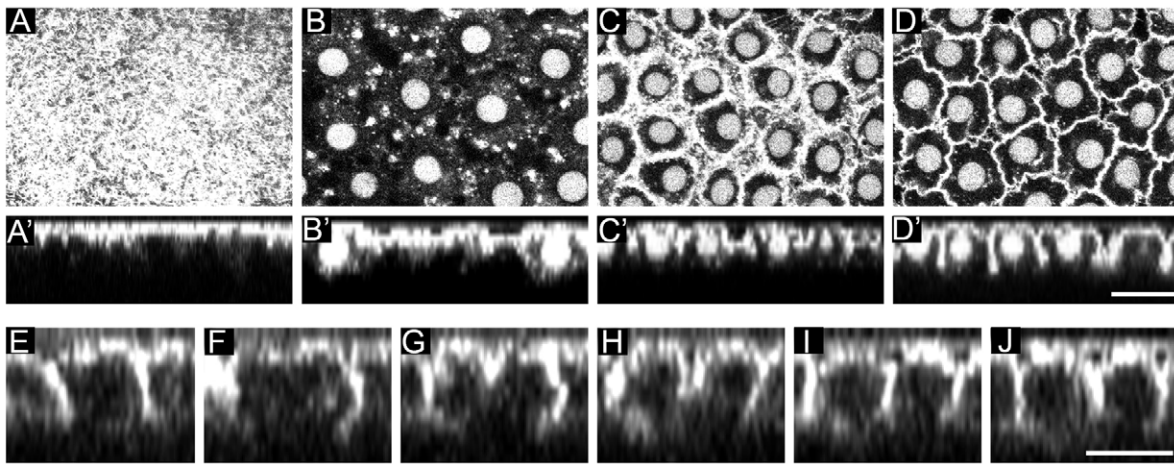
Fig. 1. Membrane ingression during cellularization. (A-D′) Time series of membrane ingression during cellularization in a nuclear-GFP transgenic *Tribolium castaneum* egg transiently expressing GAP43-YFP as a membrane marker, timed from just before nuclei reach the surface of the egg (shown in A), i.e. after the tenth nuclear division. (A-D) Optical sections at the level of the membrane (A) or at the level of the nuclei (B-D). (A′-D′) Orthogonal views from the same time points. When nuclei are not visible in the orthogonal views it is because the cross-section did not bisect them. (E-J) Time series of orthogonal views of membrane ingression during the twelfth division in a GAP43-YFP transiently labeled embryo, timed from just before division begins (as shown in D). (E) Prior to division, a single protocell is visible. (F) When the nucleus divides (not visible) the membrane moves further apart. (G) Following separation of the chromosomes (not visible), the membrane begins to invaginate between the new nuclei. (H,I) The membrane continues to invaginate between new nuclei. (J) Two new protocells are visible. Scale bars: 20 µm.

conserved cysteine residues in the extracellular protein loops and leads to the formation of a functional gap junction. However, Pannexins have also been shown to function as non-junctional channels connecting the cytoplasm with the extracellular space (Bedner et al., 2012; Scemes, 2012; Scemes et al., 2009; Shestopalov and Panchin, 2008; Sosinsky et al., 2011).

Here we show that depletion of Inx7a in *Tribolium* leads to the retraction of the invaginated membrane when basal cell closure normally starts. We propose that Inx7a forms junctions between the nascent basal membrane and the forming yolk plasmalemma, thus stabilizing the invaginated membrane and enabling basal cell closure.

RESULTS

To investigate cellularization in *Tribolium*, we followed development using live imaging of embryos in which the cell cortex was labeled with the YFP-fused, GPI-anchored plasma membrane protein GAP43 (Mavrakis et al., 2009). This fusion protein was transiently expressed by mRNA injection into eggs from wild-type beetles or from a transgenic line expressing nuclear-localized GFP (Benton et al., 2013; Sarrazin et al., 2012).

We found that the membrane invaginates between the nuclei after the tenth nuclear division (i.e. ∼t=6 h after egg lay) (Fig. 1A-D′; supplementary material Movie 1 and see also Movie 8). The eleventh division occurs 30 min later (Fig. 2A; supplementary material Movie 2). In contrast to *Drosophila*, the invaginated membrane does not retract and then invaginate anew at each nuclear division. Instead, already invaginated membrane remains at its original depth, just below the nuclei, and a new cleavage furrow invaginates between the daughter nuclei to form two protocells (Fig. 1E-J; supplementary material Movie 3). One hour after the eleventh division, the twelfth and last synchronous division takes place (Fig. 2B; supplementary material Movie 2, t=0 is set at the onset of the eleventh division in this movie).

About 90 min after this last synchronous division (at ∼t=2 h 30 min after the eleventh division), the protocells become refined into a regular array of pentagons and hexagons, with rare tetragons

and heptagons (Fig. 2D; supplementary material Movie 2). This suggests an increase in cortical tension. Concomitantly, a basal membrane starts to form (Fig. 2P,Ra-d; supplementary material Movies 4 and 5). Thus, a phase of rapid membrane extension is absent. Thirty minutes later, at ∼t=3 h, the cuboidal cells have completely closed at the basal side (supplementary material Movie 4). Finally, at ∼t=3 h 30 min, the closed cuboidal cells of the germ rudiment start to divide asynchronously for the first time, giving rise to the differentiated blastoderm stage (Fig. 2E; supplementary material Movie 2). Thus, cell closure in *Tribolium* appears to take place one cell cycle earlier than in *Drosophila*, i.e. after the twelfth instead of the thirteenth division (Handel et al., 2000; Harris et al., 2009; Lecuit, 2004; Mazumdar and Mazumdar, 2002).

In *Tribolium*, furrow canals are not enriched with actin

In *Drosophila*, the leading edges of the ingressing membrane are dilated and form interconnected furrow canals that are enriched with actin and are separated from the rest of the membrane by an Armadillo-rich BAJ (see Introduction). The live imaging with the plasma membrane marker GAP43 was not carried out at sufficient resolution to determine whether furrow canals are present in *Tribolium*. To resolve this, we inspected the tips of the ingressing membrane by TEM, and observed dilated bases (Fig. 3A-D, asterisks). Furthermore, as in *Drosophila*, these dilations are separated from the rest of the membrane by junctions (Fig. 3A-D, arrowheads). To establish if these junctions are BAJs, we used an antibody to localize Armadillo. Indeed, after the twelfth division, Armadillo localization is consistent with BAJs above the furrow canal (Fig. 3E). We conclude that furrow canals are also present in *Tribolium*.

However, in contrast to *Drosophila*, the furrow canals are not heavily enriched with actin. Neither phalloidin nor an actin antibody could detect conspicuous actin enrichment at the bases of the ingressing membrane (Fig. 3G). We did detect some basal enrichments of actin when basal cell closure starts (Fig. 3I), but these enrichments correspond only to corners where three cells meet
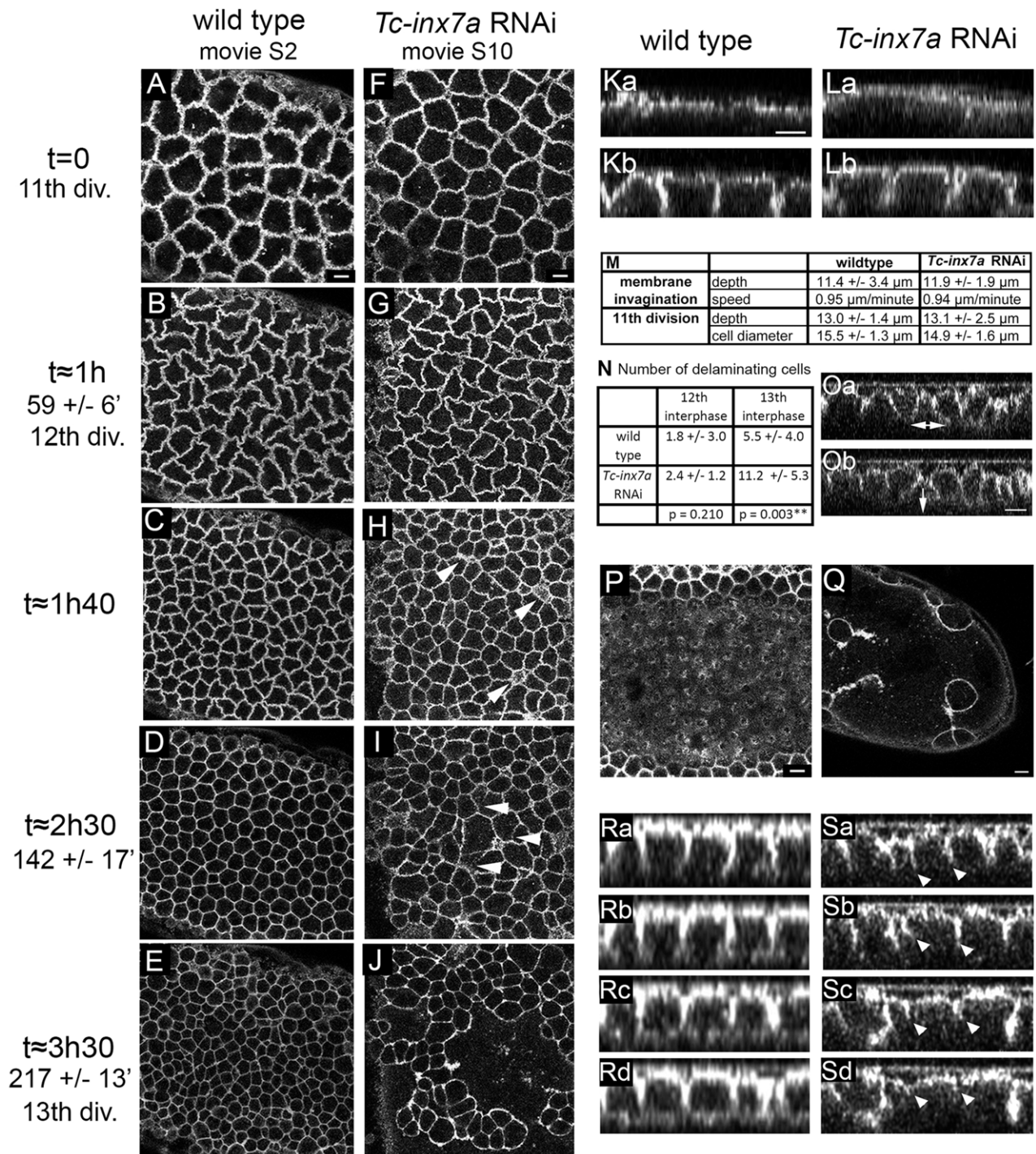
DEVELOPMENT

Fig. 2. Cellularization in wild-type and Inx7a-depleted eggs. (A-E) Stills from a time-lapse movie of a developing wild-type egg transiently expressing GAP43-YFP as a plasma membrane marker (supplementary material Movie 2). In this movie, $t=0$ is set at the onset of the eleventh division. The twelfth division ($t=1$ h) is the last synchronous division and the thirteenth ($t=3$ h 30 min) is the first asynchronous division of the germ rudiment. (F-J) Stills from a GAP43-YFP time-lapse movie of a developing $Tc-inx7a$ pRNAi egg at approximately the same time points as in A-E (supplementary material Movie 10). Arrowheads indicate delaminating protocells (H) or retracting membrane (I). (K,L) Stills from GAP43-YFP time-lapse movies showing the beginning (Ka,La) and the end (Kb,Lb) of plasma membrane ingression after the tenth division in wild-type (K; supplementary material Movie 8) and $Tc-inx7a$ pRNAi (L; supplementary material Movie 9) eggs. (M) Quantitation of the depth and speed of membrane invagination after the tenth nuclear division as well as size of the protocells after the eleventh division in wild-type and $Tc-inx7a$ pRNAi eggs (see Materials and Methods). (N) Quantification of delaminating protocells in a 145 µm×145 µm area before and after the twelfth division in eight wild-type and eight $Tc-inx7a$ pRNAi eggs. (O) Orthogonal sections showing the process of protocell delamination. During delamination, the membrane of a protocell is biased towards neighboring nuclei (Oa, double-headed arrow). This protocell is extruded from the epithelium (arrow in Ob). (P) Still from a GAP43-YFP time-lapse movie of a wild-type egg (supplementary material Movie 4) at a basal focal plane at the time of basal closure. (Q) Still from a GAP43-YFP time-lapse movie of a $Tc-inx7a$ pRNAi egg (supplementary material Movie 12). Note the large uncellularized area. (R,S) Stills from GAP43-YFP time-lapse movies showing orthogonal views of basal membrane formation in a wild-type egg (R; supplementary material Movie 5) and $Tc-inx7a$ pRNAi egg (S; supplementary material Movie 11). Arrowheads (S) indicate retracting membrane. Note that one cell on the left manages to close (Sd). Scale bars: 10 µm (the scale bar in Ka applies to all orthogonal views).
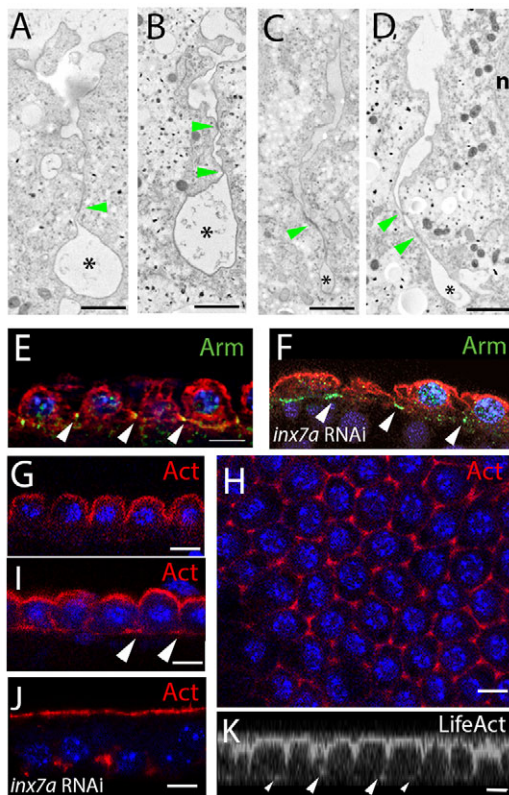
Fig. 3. Analysis of furrow canals in *Tribolium*. (A-D) TEM micrographs of the ingressing membrane in different wild-type eggs. Asterisks, furrow canals; arrowheads, junctions; n, nucleus. (E,F) Immunofluorescence (IF) visualization of Armadillo (green) and tubulin (red) and nuclear staining with DAPI (blue) in wild-type (E) and *Tc-inx7a* pRNAi (F) blastoderm. Note that in the knockdown, Armadillo is still detected on some retracting membranes (F, arrowheads). (G-J) IF visualization of actin (red) and nuclear staining with DAPI (blue) in wild-type (G-I) and *Tc-inx7a* pRNAi (J) blastoderm. No enrichment of actin is observed at the base of the ingressing membrane (G), except for the corners where three cells meet (H, arrowheads in I). A few dots of actin remain basally after *Tc-inx7a* pRNAi (J). (K) Orthogonal view of a LifeAct time-lapse movie revealing minor accumulations of actin at the bases of some of the ingressed furrows (arrowheads). Scale bars: 1 µm in A-D; 10 µm in E-K.

(Fig. 3H) and, as more membrane is present at these points, this apparent actin accumulation is likely to reflect normal levels of cortical actin. In order to exclude the possibility of penetration problems of the actin antibody, we also injected mRNA encoding LifeAct-GFP, which specifically labels F-actin (Benton et al., 2013; Riedl et al., 2008). Similar to the actin antibody, this revealed minor actin accumulation at the base of some of the ingressed furrows (Fig. 3K), but incomparable to the well described and consistent localization of actin to all furrow canals in *Drosophila* (Warn and Magrath, 1983).

Taken together, these results suggest that furrow canals are formed during *Tribolium* cellularization but that they are less enriched with actin than those in *Drosophila*.

Novel junctions form along the nascent basal membrane

After the twelfth division, the dilated edges of the ingressed membrane start to enlarge (Fig. 4A-D). Subsequently, the ingressed membrane splits at the basal side as the furrow canals flatten (Fig. 4E,F). Surprisingly, we found that new junctions form between the nascent basal membrane and the forming yolk plasmalemma (Fig. 4E,F, red arrowheads). As the basal membrane extends laterally, additional junctions are continuously added, until junctions are present along the

whole basal membrane (Fig. 4G; supplementary material Fig. S1). Such junctions have not been described in *Drosophila*.

In *Drosophila*, cell closure is mediated by actin ring constriction (reviewed by Harris et al., 2009). Although we could detect these rings by immunofluorescence in *Drosophila* (supplementary material Fig. S1F), we could not detect an equivalent in *Tribolium*. To exclude the possibility of penetration difficulties of the antibody, we also analyzed basal cell closure by live imaging of embryos transiently expressing LifeAct-GFP (Fig. 4H,J,L,N). During basal membrane formation, a fine network of actin becomes visible at the base of the forming cells (Fig. 4H; supplementary material Movie 6). An overlay of a more apical view revealed enrichments of actin at the constrictions of the basal membrane in some protocells (Fig. 4J,L, see Fig. 4N for a lateral view). However, these enrichments are incomparable to the obvious actin rings in *Drosophila* (supplementary material Fig. S1F) and closely reflect the pattern observed with the membrane marker GAP43-YFP (Fig. 2P). This suggests that these actin enrichments represent normal levels of cortical actin, and that the role of the actin cytoskeleton in basal cell closure might not be as prominent as in *Drosophila*.

We did, however, detect an enrichment of microtubules at the basal side of the closing cells (Fig. 4P,R). Microtubules are also evident in TEM micrographs (Fig. 4B,D,F). Thus, it is possible that polarized membrane insertion along microtubules plays a role in basal cell closure, similar to that seen during the phase of rapid membrane extension in *Drosophila*. Consistent with this, we observed numerous highly mobile GAP43-YFP-positive compartments, suggesting extensive membrane activity (supplementary material Movie 7; Fig. 4T). Furthermore, at the basal sides of the forming cells, TEM revealed conspicuous vesicles with a thin membrane and remnants of homogenous filling (Fig. 4C,E, black arrowheads). These are probably lipid droplets that could supply lipids for membrane synthesis. However, we did not functionally test a possible role for membrane insertion in basal cell closure.

Taken together, basal cell closure in *Tribolium* relies on different mechanisms than those that operate in *Drosophila*. First, the actin pattern found in *Tribolium* is incomparable to the conspicuous actin rings detected in *Drosophila* during basal constriction. Second, junctions form between the nascent basal membrane and the forming yolk plasmalemma. As we do not detect Armadillo at the basal membrane (supplementary material Fig. S1E), these junctions are unlikely to be adherens junctions.

TC011061 is an *Innexin 7* ortholog and its maternal knockdown leads to a strong defect in cellularization

In an attempt to identify the nature of the basal junction during cellularization in *Tribolium castaneum*, we performed a small-scale pRNAi screen targeting candidate junction proteins (Bucher et al., 2002). Knockdown of most genes encoding these proteins generated either sterile mothers (such as the E-cadherin knockdown) or mild non-penetrant egg phenotypes (supplementary material Table S1). By contrast, injection of double-stranded (ds) RNA targeting TC011061, a gene with clear similarities to Innexins, led to a consistent and 100% penetrant phenotype in the early development of all eggs. In these eggs, late blastoderm stage nuclei are irregularly spaced when compared with wild-type eggs (Fig. 5A-D). Phalloidin staining marking the cell cortex indicates the absence of membrane between many of the nuclei (Fig. 5E-H), giving the impression of multinucleated cells. Furthermore, some nuclei detach from the apical surface (Fig. 5F). These phenotypes are characteristic of cellularization mutants in *Drosophila* (Mazumdar and Mazumdar, 2002).
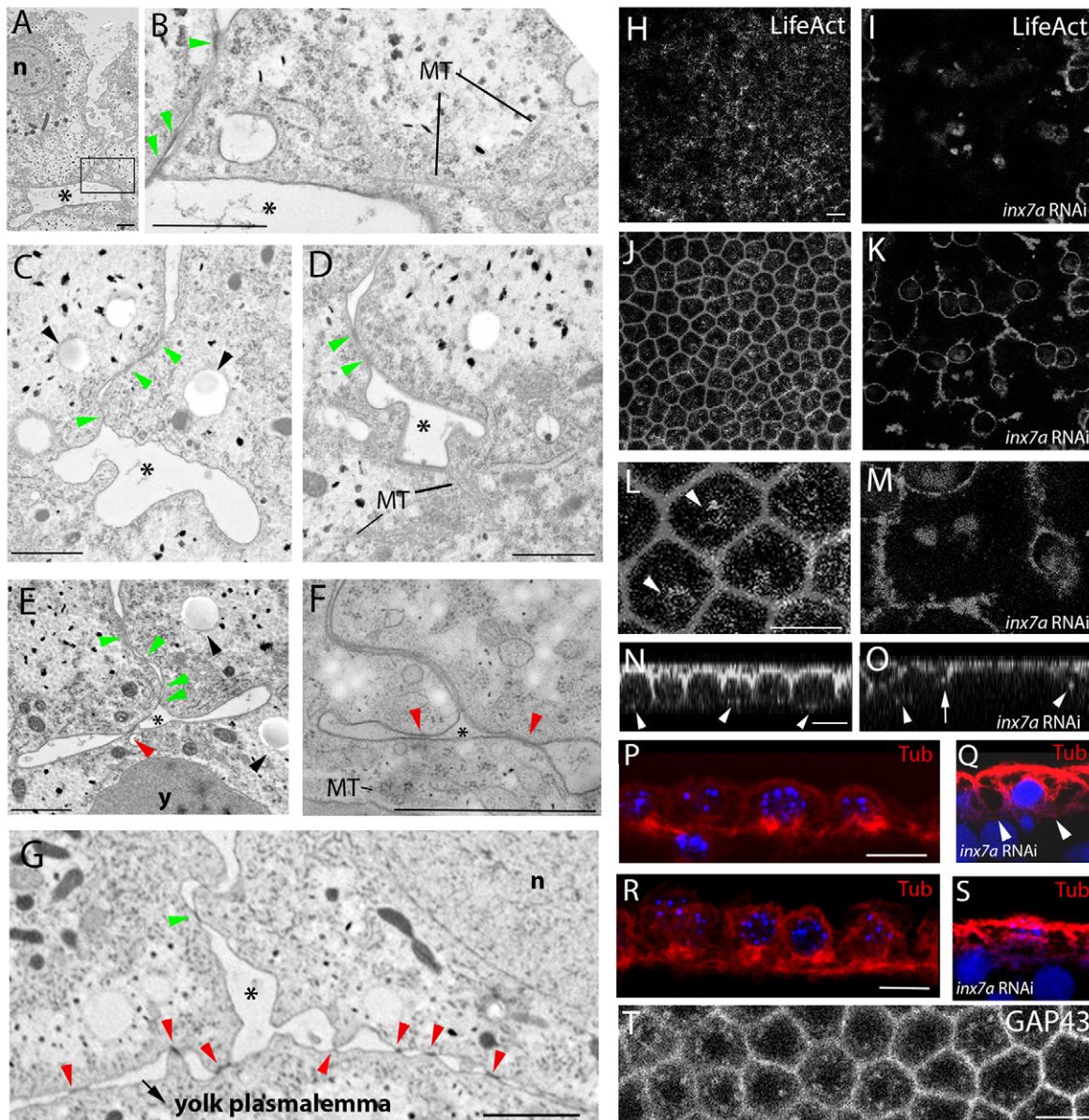
Fig. 4. Basal cell closure in *Tribolium*. (A-D) TEM micrographs showing examples of the enlarging and splitting furrow canals (asterisks). (B) Magnification of the area boxed in A. (E-G) TEM visualization of both the lateral BAJs (green arrowheads) as well as the novel junctions between the nascent basal cell membrane and the forming yolk plasmalemma (red arrowheads; see also supplementary material Fig. S1). Black arrowheads, vesicles. Asterisks indicate the split furrow. n, nucleus; MT, microtubuli; y, yolk. (H,I) Still from LifeAct-GFP time-lapse movies in wild type (H) and after *Tc-inx7a* pRNAi (I) at a basal focal plane. Note that the extensive basal network of actin seen in wild type (H) is absent in the knockdown (I). (J,K) Overlay of a more apical plane on the stills shown in H and I. (L,M) Magnification of J and K. Arrowheads (L) point at accumulations of actin where the cells constrict. (N,O) Orthogonal views of J and K, respectively. Arrowheads (N) indicate the presence of actin where the cells constrict. Arrow (O) indicates retracting membrane, with arrowheads indicating remaining dots of actin. (P-S) IF visualization of tubulin around nuclei in wild-type (P,R) and *Tc-inx7a* pRNAi (Q,S) blastoderms presented as an overlay of several confocal planes. Nuclei are stained with DAPI (blue). Note that in wild-type eggs, microtubules appear enriched and condensed during basal cell closure, whereas they retract in *Tc-inx7a* pRNAi (S). Arrowheads (Q) indicate basal tubulin. (T) Still from GAP43-YFP live imaging (supplementary material Movie 7) showing numerous moving compartments at the basal side of the forming cell. Scale bars: 1 µm in A-G; 10 µm in H-T.

In total we found eight Innexin genes in the *Tribolium* genome, all encoding proteins with the conserved four-TM topology, a characteristic YYQW motif in the second TM domain, and the two conserved C residues (supplementary material Fig. S2) (Bauer et al., 2005; Phelan, 2005). To establish the correct orthology of TC011061 and the other Innexin genes, we first generated a maximum likelihood phylogeny including arthropod Innexins from available full genome sequences (Fig. 6). Although the bootstrap values at the base of the tree are low, the crustacean and insect Innexins strongly cluster together in clear orthology groups,

allowing unambiguous classification of the *Tribolium* Innexins. As in *Drosophila*, single orthologs of *innexin1* (*ogre*), *innexin2* (*kropf*) and *innexin3* are present in *Tribolium*. Whereas the *Drosophila* genome contains the paralogs *innexin 4* (*zpg*), *Innexin 5* and *Innexin 6*, *Tribolium* possesses a single ortholog that we named *Tc-inx456*. In the 3.0 version of the *Tribolium* genome, two *innexin8*-like genes are predicted (TC011065 and TC011066), but upon closer inspection these belong to a single gene that produces two isoforms with different first exons, similar to the *Drosophila innexin8 shakB* locus (Phelan and Starich, 2001). Finally, our
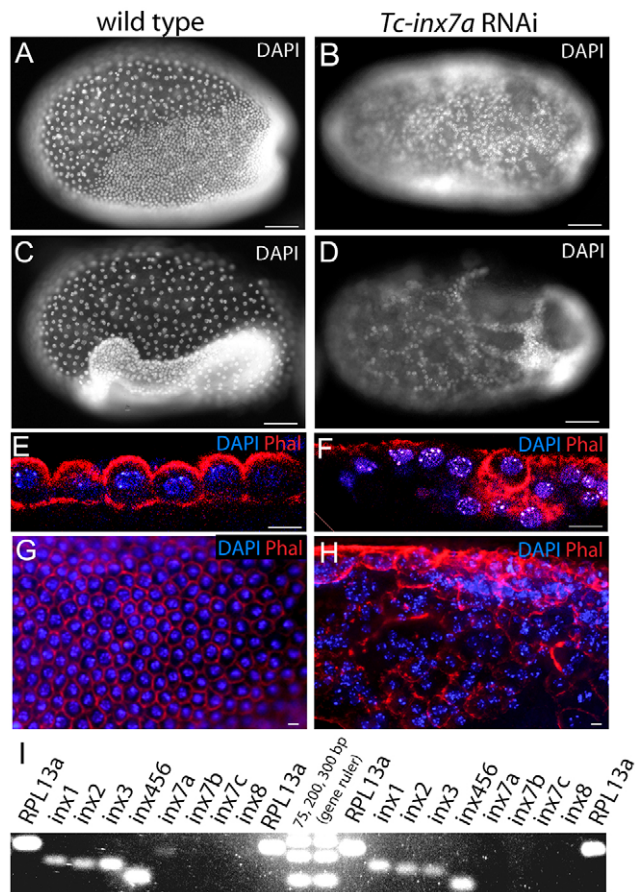
DEVELOPMENT

Fig. 5. Knockdown of *Tc-inx7a* leads to a strong cellularization phenotype. (A-D) Visualization of nuclei with DAPI of wild-type (A,C) and *Tc-inx7a* pRNAi (B,D) differentiated blastoderms (A,B) and at early gastrulation (C,D). Note that the nuclei are irregularly spaced in the knockdown (B,D). (E-H) Visualization of nuclei (DAPI, blue) and actin marking the cell cortex (phalloidin, red) in wild-type (E,G) and *Tc-inx7a* pRNAi (F,H) eggs by confocal (E,F) and epifluorescence (G,H) microscopy (in H, the epifluorescent image has been deconvoluted). Note that cortical actin is absent between most nuclei in the knockdown (F) and the presence of apparently multinucleated cells (H). (I) RT-PCR on cDNA from 0- to 6-h-old eggs from wild-type (lanes left of size marker) and *Tc-inx7a* dsRNA-injected (lanes right of size marker) mothers. *Tc-inx7a* is weakly expressed in wild-type eggs, and this expression is absent in *Tc-inx7a* pRNAi eggs. *Ribosomal protein 13a* (*RPL13a*) was used as reference gene (Lord et al., 2010). See supplementary material Table S2. Scale bars: 50 µm in A-D; 10 µm in E-H.

phylogenetic analysis clearly identified TC011061 as an *Innexin 7* ortholog (bootstrap value=93), that we arbitrarily named *Tc-inx7a*, as the *Tribolium* genome contains two other *innexin7* paralogs (named *Tc-inx7b* and *Tc-inx7c*). These three genes are close together in a head-to-tail orientation on the chromosome, and their phylogeny suggests that they are *innexin7* duplications specific to the *Tribolium* lineage.

To verify the efficiency and specificity of *Tc-inx7a* knockdown, we used two other non-overlapping *Tc-inx7a* dsRNA fragments and confirmed in each case the absolute penetrance of the phenotype (100% of the eggs showed strong cellularization defects). Next, using qPCR, we quantified the expression of all Innexin genes in the wild type and in the three different *Tc-inx7a* pRNAi treatments (supplementary material Table S2). We found strong expression of *Tc-inx7a* in wild-type ovaries, which was reduced by 84% with pRNAi, whereas expression of the other Innexin genes was not affected, validating specificity (supplementary material Table S2). In

early eggs, we found weak expression of *Tc-inx7a*, but this expression was completely absent after *Tc-inx7a* pRNAi (see also Fig. 5I). This confirms the efficiency of the knockdown.

Although still present at moderate levels, *Tc-inx3* expression is also reduced in early *Tc-inx7a* pRNAi eggs (Fig. 5I; supplementary material Table S2), and so the possibility remains that the phenotype we observe results from a reduction in *Tc-inx3* expression. To test the involvement of *Tc-inx3* expression in the cellularization phenotype, we specifically targeted *Tc-inx3* by pRNAi. This resulted in 94% reduction of the *Tc-inx3* mRNA level (whereas the other Innexins are not strongly affected; supplementary material Table S2) but, crucially, did not lead to the phenotype described for *Tc-inx7a* pRNAi. We are therefore confident that the cellularization phenotype that we describe is exclusively due to the loss of Inx7a.

Lastly, the cellularization defects upon *Tc-inx7a* RNAi were observed after pRNAi, i.e. after knockdown of both maternal and zygotic transcription of *Tc-inx7a*. To establish which mRNA pool is important for cellularization, we injected *Tc-inx7a* dsRNA into 0- to 2-h-old eggs. We observed a consistent, albeit later, phenotype in dorsoventral patterning and gastrulation but no cellularization phenotype (data not shown). We therefore conclude that the cellularization phenotype depends on the maternal expression of *Tc-inx7a*.

Taken together, TC011061 is an *Innexin 7* ortholog and its parental knockdown leads to a strong and consistent phenotype in cellularization.

Inx7a is required to maintain the invaginated membrane after the twelfth division

To investigate how this phenotype arises, we compared cellularization of *Tc-inx7a* knockdown eggs with the wild type using GAP43-YFP live imaging. In *Tc-inx7a* pRNAi eggs, both the depth and speed of membrane invagination at the tenth division are unaltered (Fig. 2K-M; supplementary material Movies 8 and 9). Similarly, at the eleventh division, no differences in the depth of the cleavage furrows or diameter of the protocells are observed between wild-type and *Tc-inx7a* pRNAi eggs (Fig. 2F,L,M; supplementary material Movie 10).

The dramatic phenotype upon *Tc-inx7a* pRNAi starts to develop after the twelfth division. First, directly after this last synchronous division, some protocells delaminate from the epithelium (arrowheads in Fig. 2H; supplementary material Movie 10). This also occurs to a small extent before the twelfth division, but not significantly more often than in wild type (Fig. 2N). After the twelfth division, however, Inx7a-depleted eggs show a highly significant increase in the number of delaminating protocells, suggesting a general instability of the blastoderm. During delamination, the membrane of a protocell becomes skewed towards neighboring nuclei (Fig. 2Oa), ending in extrusion of that protocell (Fig. 2Ob). Second, ingressed membrane between the protocells strikingly disappears by the time basal cell closure starts in wild-type eggs (arrowheads in Fig. 2S; supplementary material Movie 10). Orthogonal views reveal that this disappearance is in fact a retraction of invaginated membrane to the apical surface (arrowheads in Fig. 2S; supplementary material Movie 11). This leads to a complete reversal of the cellularization process and gives rise to large cell-free areas (Fig. 2J; supplementary material Movie 10). In the most extreme cases, close to 100% of the invaginated membrane retracts (Fig. 2Q; supplementary material Movie 12) and only a few cells have closed basally (Fig. 2Q,S; supplementary material Movie 12). In conclusion, in the absence of Inx7a, plasma membrane invaginates normally but retracts when basal cell closure starts.
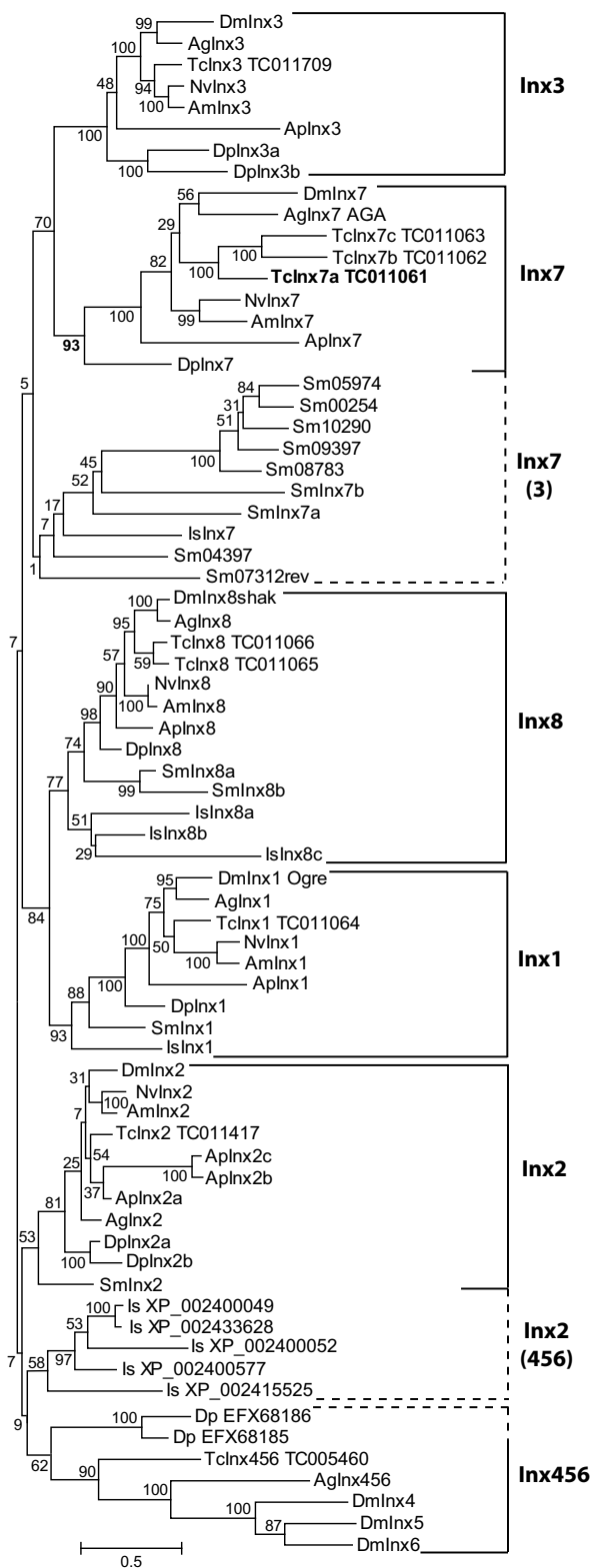
Fig. 6. Maximum likelihood phylogeny of the arthropod Innexins. Amino acid substitution model WAG+I+G (see Materials and Methods). Root was placed arbitrarily. Bootstrap values of 1000 replicates are indicated as percentage. The duplications of the pea aphid *inx2* genes confuse the Inx2 branch somewhat. Sm, centipede *Strigamia maritima*; Is, mite *Ixodes scapularis*; Dp, water flea *Daphnia pulex*; Ap, pea aphid *Acyrthosiphon pisum*; Am, bee *Apis mellifera*; Nv, wasp *Nasonia vitripennis*; Tc, beetle *Tribolium castaneum*; Ag, mosquito *Anopheles gambiae*; Dm, fly *Drosophila melanogaster*. *Strigamia maritima* numbers are predictions from the preliminary genome sequence. SmInx7a and SmInx7b are named based on synteny in a gene cluster that is incorrectly predicted as one fused gene Sm07312 but in fact consists of SmInx2, SmInx7a, SmInx7b, Inx1 and Inx8a. This synteny is also found in other arthropods, such as *Nasonia*, and seems to be ancestral. Inx3-like sequences would then have arisen in the Pancrustacea. Sm08783, Sm09397, Sm10290, Sm00254, Sm05974 and possibly Sm04397 might be duplications of Inx7, but low bootstrap values do not allow unambiguous identification. Sm07312rev is an Inx7-like gene that has an inverted orientation in the Sm07312 cluster. Sm10724 is a duplication of Inx8a and is named SmInx8b. The mite sequences XP_002415525, XP_002400577, XP_002400052, IsXP002433628 and 002400049 cluster together with Inx456, but could as well belong to the Inx2 group; the latter would be more likely given the presence of Inx2 in the ancestral cluster. The *Daphnia* sequences EFX_18186 and EFX_68185 cluster together with Inx456. Since this could be due to long branch attraction, these sequences have not been named. Inx456 could thus have arisen in the higher holometabolous insects.

RNAi knockdown eggs and even persists on the retracting membrane (Fig. 3F). This suggests that Inx7a is not required for BAJ formation and maintenance. Microtubules also appear in the basal part of the cell in Inx7a-depleted eggs (Fig. 4Q), suggesting that Inx7a does not affect the initial formation of the basal microtubules. However, these microtubules never become as prominent as in wild type, and later retract with the retracting membrane (Fig. 4S). Given the normal initial formation of microtubules, it is possible that this tubulin retraction is a consequence of the retraction of the membrane rather than its cause. Thus, we could find no evidence that incorrect localization of BAJs or microtubules causes the retraction of the ingressed plasma membrane.

In *Drosophila* cellularization mutants, such as *discontinuous actin hexagon* (*dah*) or *nullo*, membrane retraction is precipitated by reduced levels of F-actin at the furrow canals (Sokac and Wieschaus, 2008b; Zhang et al., 1996). As interactions between the actin cytoskeleton and gap junction proteins have been shown for Connexin 43 (Crespin et al., 2010; Wall et al., 2007) and the Pannexins (Bhalla-Gehi et al., 2010), we hypothesized that actin might be incorrectly localized upon *Tc-inx7a* pRNAi. Indeed, a basal network of actin does not appear to form in Inx7a-depleted eggs (Fig. 4I,K,M,O; supplementary material Movie 13). In Inx7a-depleted eggs, actin is visible at the cortex of the few cells that do manage to close (Fig. 4K,M,O), at the retracted membrane (Fig. 4O) and in a few basal dots (Fig. 3J and Fig. 4K,M,O). However, no differences in actin localization are observed between Inx7a-depleted and wild-type eggs until basal cell closure should start. The possibility thus remains that the absence of the basal actin network is merely a consequence of the missing basal membrane, rather than its cause.

Overall, Inx7a is required for the stabilization of the ingressed membrane once basal membrane formation begins. We could find no evidence, however, that Inx7a exerts its function by directly localizing BAJs, microtubules or actin.

Inx7a-V5 localizes to the basal membrane

Next, we hypothesized that Inx7a is a component of the junctions identified by TEM between the forming basal membrane and the

No evidence for a direct role of Inx7a in BAJ, tubulin or actin localization

As Innexin 2 in *Drosophila* colocalizes and interacts with Armadillo (Bauer et al., 2004), we hypothesized that BAJ formation might be affected upon loss of Inx7a, causing destabilization of the ingressed membrane. However, Armadillo localizes normally in *Tc-inx7a*
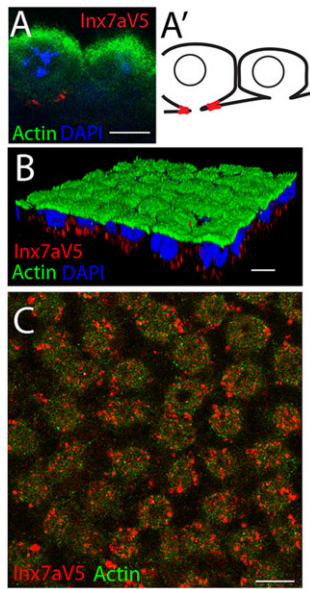
Fig. 7. Localization of the transiently expressed Inx7a-V5 fusion protein.
(A-C) IF localization of transiently expressed Inx7a-V5 (with anti-V5 antibody, red), actin (with anti-actin antibody, green) and nuclei (DAPI, blue).
(A) Orthogonal confocal section, showing that Inx7a-V5 localizes to the base of the invagination where the membrane of the nascent cell and the yolk plasmalemma meet. (A′) Schematic interpretation of A. (B) 3D opaque reconstruction showing the basal localization of Inx7a-V5. Fixation was optimized for V5 antibody staining, resulting in poor actin antibody penetration that was insufficient to visualize the basal membrane. (C) Confocal section through the base of the forming cells where Inx7-V5 is detected in plaques, mostly overlapping with the basal cortical actin. Scale bars: 10 μm.

yolk plasmalemma. These junctions could flatten and split the enlarged furrow canal, thus stabilizing the ingressed membrane. In order to test this hypothesis, we needed to visualize the localization of Inx7a protein. As the antibody against *Drosophila* Innexin 7 recognizes a peptide stretch that is not present in *Tribolium* Inx7a (supplementary material Fig. S2), we designed an Inx7a-V5 fusion protein, injected its mRNA into early wild-type eggs and performed immunohistochemistry using an antibody against the V5 tag. The transiently expressed protein was detected in 15 out of 45 injected eggs and was indeed localized at the base of the invaginated membrane (Fig. 7A). This localization is observed when the tip of the invaginated membrane starts to enlarge and split between the cells (Fig. 7A). This stage coincides with the delaminating protocells following *Tc-inx7a* pRNAi. Finally, during actual basal cell closure, Inx7a-V5 localizes all over the forming basal membrane in plaques typical for gap junctions (Shestopalov and Panchin, 2008) (Fig 7B,C). This stage coincides with the retraction of the membranes following *Tc-inx7a* pRNAi. We propose that Inx7a forms gap junctions between the nascent basal cell membrane and the yolk plasmalemma, stabilizing the forming basal membrane.

DISCUSSION
We have described cellularization in the beetle *Tribolium castaneum* and identified junctions joining together the laterally extending basal membrane and the forming yolk plasmalemma. In a functional screen for junction proteins, we identified a crucial role for Inx7a in cellularization. When *Tc-inx7a* is depleted maternally, the basal cell membranes do not form and the ingressed plasma membrane retracts to the apical surface at the time basal cell closure

starts. We propose that Inx7a is a component of the newly identified junctions that stabilize the ingressed membrane.

Differences between *Tribolium* and *Drosophila* cellularization
Cellularization in *Tribolium* exhibits six remarkable differences to that in *Drosophila*. First, the plasma membrane does not retract during divisions, unlike in *Drosophila*. Second, cell closure in *Tribolium* appears to take place one cell cycle earlier than in *Drosophila*, i.e. after the twelfth instead of the thirteenth division (Handel et al., 2000; Harris et al., 2009; Lecuit, 2004; Mazumdar and Mazumdar, 2002). This difference is not surprising, as variation in the number and rate of nuclear divisions is common among insect groups (Anderson, 1972). Third, the furrow canals are not enriched with actin.

Fourth, in *Drosophila*, the phase of slow membrane extension is accompanied by elongation of the nuclei and is followed by a phase of rapid membrane extension allowing deep ingression before final closure of the cell (Schejter and Wieschaus, 1993). In *Tribolium*, the nuclei remain spherical, and the rapid phase is absent. After the last synchronous division, the membrane does not extend any further (Fig. 8A) and cell closure directly follows (Fig. 8B,C), leading to a much thinner blastoderm with cuboidal cells. Cells of the embryonic ectoderm then elongate and form a pseudostratified columnar epithelium (Benton et al., 2013; Handel et al., 2005). This is similar to most insect lineages thus far studied, including basally branching insects, and is therefore likely to be ancestral (Anderson, 1972; Ede, 1964). By contrast, a thickened layer of cytoplasm with apically positioned nuclei has evolved in *Drosophila* and other Cyclorrhapha (higher Diptera) (Bullock et al., 2004). Thus, the membrane has to ingress much further, requiring a long phase of rapid extension. As a result, cellularization in *Drosophila* directly yields columnar cells. This might facilitate more rapid development, as it has been suggested that cuboidal cells have to elongate before gastrulation, whereas columnar cells can directly enter gastrulation (Bullock et al., 2004).

Fifth, basal cell closure appears to take place through different mechanisms in *Drosophila* and *Tribolium*. Interestingly, in *Drosophila*, basal cell closure is mediated by contractile actin rings (Harris et al., 2009). We could not visualize such rings in *Tribolium* using either LifeAct-GFP live imaging or immunohistochemistry with an anti-actin antibody, whereas the latter method did reveal these rings in *Drosophila* (supplementary material Fig. S1F). The microtubules visible in TEM micrographs and tubulin antibody stainings, and the moving GAP43-positive vesicles, suggest that polarized membrane insertion might be a driving force involved in basal cell closure in *Tribolium*, similar to the fast phase of membrane extension in *Drosophila*. However, the exact forces involved in basal cell closure in *Tribolium* remain to be elucidated.

Sixth, we found junctions that keep together the forming basal membrane and the forming yolk membrane. Such junctions have not been described in *Drosophila*. It seems that these junctions are instrumental in basal cell closure in *Tribolium*.

The function of Inx7a
The phenotype upon *Tc-inx7a* knockdown demonstrates a role for Inx7a in stabilization of the ingressed plasma membrane after the twelfth nuclear division. Furthermore, the localization of Inx7a-V5 suggests that Inx7a forms the newly identified junctions between the forming basal membrane and the yolk membrane. We propose that these Inx7a-based junctions convey stability to the ingressed plasma membrane in two ways. First, they split the leading edges (furrow canals) of the ingressed membrane immediately after the twelfth
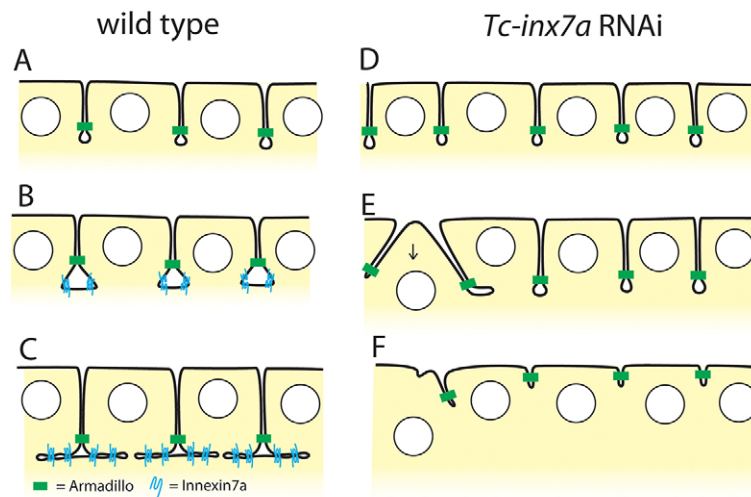
Fig. 8. Model for a role of Inx7a in cellularization in *Tribolium*. (A-C) Wild-type cellularization. (A) The plasma membrane invaginates between the nuclei after the tenth nuclear division and remains at this depth. Furrow canals and basal adherens junctions (BAJs) containing Armadillo (green) form. (B,C) Inx7a forms junctions in the enlarging furrow canal, mediating the splitting of the tip of the ingressed membrane (C). Inx7a forms gap junctions joining together the nascent basal cell membrane and the forming yolk plasmalemma, stabilizing the ingressed membrane and enabling basal cell closure. (D-F) *Tc-inx7a* pRNAi severely impacts cellularization. (D) The plasma membrane invaginates normally in *Tc-inx7a* pRNAi embryos and BAJs containing Armadillo (green) form. (E) In the absence of Inx7a, the tip of the ingressed membrane does not split properly. The ingressed membrane of a protocell can be inclined towards neighboring nuclei; this particular protocell will be extruded from the epithelium (arrow). (F) Finally, ingressed membrane retracts to the apical surface, as the membrane is not stabilized.

division (Fig. 8B). In the absence of proper splitting, the membrane of a protocell can become skewed towards neighboring nuclei, as occurs during protocell delamination (Fig. 8E). Second, these junctions stabilize the forming basal membrane during the phase of actual basal cell closure (Fig. 8C). Absence of this stabilization leads to the retraction of the ingressed membrane to the apical surface (Fig. 8F), causing a complete reversal of the cellularization process.

As Innexin 7 is a gap junction protein, we suggest that the newly identified junctions are gap junctions and that Inx7a is a key component of them. However, this remains to be proven, as Innexins can also function in a hemichannel (Scemes et al., 2009). It is also possible that the newly identified junctions are of a completely different nature, and that Inx7a is merely involved in their initial assembly or stabilization.

It might seem surprising that the sole depletion of Inx7a shows this strong cellularization phenotype given that *Tc-inx1*, *Tc-inx2*, *Tc-inx3* and *Tc-inx456* are also expressed during cellularization. However, specific properties might distinguish Inx7a from the other expressed Innexins. For instance, Inx7a displays a distinctive Trp196 at the beginning of TM3 (supplementary material Fig. S2), a position involved in the oligomerization compatibility of vertebrate Connexin 43 (Lagrée et al., 2003). This Trp residue is also conserved in *Nasonia*, *Apis* and *Anopheles* Inx7. It is also possible that Inx7a primes and stabilizes the formation of heteromeric gap junctions with other Innexins. This has been proposed for *Drosophila* Inx3 in an Inx1-Inx2-Inx3 complex in the amnioserosa, as the sole loss of Inx3 leads to a strong dorsal closure phenotype, in contrast to the individual loss of Inx1 or Inx2 (Giuliani et al., 2013).

The proposed mechanism of basal cell closure involving Inx7a could be unique to *Tribolium*. However, since the *Drosophila* mode of cellularization involving columnar cells is evolutionarily derived, it seems more likely that the Inx7-mediated process is ancestral.

MATERIALS AND METHODS
Time-lapse movies
One- to two-hour-old eggs were dechorionated in 0.5% hypochlorite solution, mounted and injected with 3 µg/µl GAP43-YFP or LifeAct-GFP mRNA as described by Benton et al. (2013). They were then left to develop for 3-4 h under Voltalef 10S hydrocarbon oil at 32°C, and imaged at 32°C with a Leica SP5 inverted confocal laser microscope using the 40× or 63× objective (Benton et al., 2013). In total, we analyzed movies of 22 wild-type and eight *Tc-inx7a* pRNAi eggs. For Fig. 2N, statistical significance was assessed using Student's *t*-test. Six to nine cells per movie were followed and measured in detail for Fig. 2M.

Transmission electron microscopy
Eggs were incubated in 10% BSA (as a cryoprotectant) and high-pressure freezing was performed with a Leica EM PACT2, followed by freeze substitution. Specimens were embedded in Agar 100 resin (Agar Scientific, AGR1031), sectioned and examined with a JEOL 1010 transmission electron microscope.

Egg fixation and immunohistochemistry
Eggs were fixed in a 1:1 mix of 4% formaldehyde and heptane, devittelinized with a methanol shock, and stored in methanol. Anti-β-catenin/Armadillo (Panfilio et al., 2013), anti-actin (Sigma, A2066) or anti-V5 (Invitrogen, R960) antibodies were used 1:1000, 1:50 or 1:1000, respectively, in PBS supplemented with 1% BSA (PBS-BSA) overnight at 4°C. After washing, eggs were incubated with anti-rabbit Alexa Fluor 488 (Life Technologies, A-11008) at 1:250 in PBS-BSA. For actin staining using phalloidin, eggs were fixed in 4% paraformaldehyde for 15 min and devittelinized using forceps and needle before incubation with 1:5000 Alexa Fluor 568-conjugated phalloidin (Life Technologies, A12380) for 20 min at room temperature. Eggs were mounted in Vectashield with DAPI (Vector Laboratories, H-1500) and imaged under a Leica DM6000 epifluorescence, SP5 or SPE confocal microscope.

Quantitative (q) PCR
Total RNA was extracted using Trizol (Invitrogen) followed by DNA digestion and column purification using the RNeasy Kit (Qiagen). First-strand cDNA was made using the Cloned AMV First-Strand Synthesis Kit (Invitrogen). qPCR reactions were carried out using the SYBR Green I Kit (Eurogentec) on a CFX96 thermocycler (Bio-Rad) as: 95°C for 15 s, 60°C for 30 s, 72°C for 30 s; followed by dissociation analysis of a ramp from 65°C to 95°C with a read every 0.5°C. qPCR primers (supplementary material Table S3) were designed such that they spanned a large intron or overlapped an exon boundary, except for *inx2*, which has no introns.

RNAi
dsRNA was synthesized using SP6 and T7 RNA polymerases (Ambion) and injected into pupae according to Bucher et al. (2002) for pRNAi (see supplementary material Table S1 for details and Table S3 for *inx7a* RNAi primer sequences). Injection of dsRNA into eggs was performed as previously described for mRNA injection (Benton et al., 2013).

Phylogenetic analysis
Putative orthologs were identified by BLAST (Altschul et al., 1997). Alignment was made using Praline (http://www.ibi.vu.nl/programs/pralinewww). The parts of the alignment where most sequences had gaps were not taken into account for phylogenetic analysis by creating a mask in Seaview (Galtier et al., 1996). WAG+I+G was the most informative amino acid substitution model according to Prottest (Abascal et al., 2005). The

maximum likelihood phylogeny was generated using PhyML (Guindon and Gascuel, 2003) and was edited in MEGA3.1 (Kumar et al., 2004). National Center for Biotechnology Information (NCBI) accession numbers of the sequences used (see Fig. 6 for species abbreviations) are: XP_002405917, IsInx1; XP_002415523, IsInx2; XP_002405920, IsInx8a; XP_002433826, IsInx8b; XP_002434835, Inx8c; EFX65318.1, DpInx1; EFX65316.1, DpInx2a; EFX77054.1, DpInx2b; EFX74755.1, DpInx3a; EFX74754.1, DpInx3b; EFX65317.1, DpInx7; EFX84089.1, DpInx8; XP_001946431, ApInx1; XP_001944681, ApInx2a; XP_003241809, ApInx2b; XP_001947982, ApInx2c; XP_001949382, ApInx3; XP_003247903.1, ApInx7; XP_001944798, ApInx8; XM_001121323, AmInx1; XM_003251623, AmInx2; XM_623560, AmInx3; XM_624661, AmInx7; XM_396916, AmInx8; XP_001603984, NvInx1; XP_001604034, NvInx2; XM_003427685, NvInx3; XM_001603958, NvInx7; XP_001599753, NvInx8; AGAP001476-PA, AgInx1; AGAP001488-PA, AgInx2; AGAP004510-PA, AgInx3; AGAP006241-PA, AgInx456; AGAP001477-PA, AgInx7; AGAP001487-PB, AgInx8.

Inx7a-V5 transient expression

The full coding sequence of Inx7a was cloned using primers 5′-AGAATTCACATGTTGAAAACTTTCGAAGCG-3′ and 5′AACTCG-AGGTCAAATTTCGCCGGCTTTTTC-3′, digested with *Eco*RI and *Xho*I, and ligated into pMT/V5 (Invitrogen) that had been digested with the same enzymes. The fusion construct was excised with *Pci*I and *Not*I, cloned into the modified expression vector pT7-DsRed (Benton et al., 2013), linearized with *Not*I, and *in vitro* transcribed using the T7 mMESSAGE mMACHINE Kit (Ambion). Capped mRNA (3 µg/µl) was injected into 0- to 2-h-old eggs. Eggs were allowed to develop for 8 h at 32°C and fixed for staining with the anti-V5 antibody.

References

Abascal, F. and Zardoya, R. (2013). Evolutionary analyses of gap junction protein families. *Biochim. Biophys. Acta* **1828**, 4-14.

Abascal, F., Zardoya, R. and Posada, D. (2005). ProtTest: selection of best-fit models of protein evolution. *Bioinformatics* **21**, 2104-2105.

Acharya, S., Laupsien, P., Wenzl, C., Yan, S. and Grosshans, J. (2014). Function and dynamics of slam in furrow formation in early Drosophila embryo. *Dev. Biol.* **386**, 371-384.

Alexopoulos, H., Böttger, A., Fischer, S., Levin, A., Wolf, A., Fujisawa, T., Hayakawa, S., Gojobori, T., Davies, J. A., David, C. N. et al. (2004). Evolution of gap junctions: the missing link? *Curr. Biol.* **14**, R879-R880.

Altschul, S. F., Madden, T. L., Schäffer, A. A., Zhang, J., Zhang, Z., Miller, W. and Lipman, D. J. (1997). Gapped BLAST and PSI-BLAST: a new generation of protein database search programs. *Nucleic Acids Res.* **25**, 3389-3402.

Anderson, D. T. (1972). The development of holometabolous insects. In *Developmental Systems: Insects* (ed. S. Counce and C. Waddington), pp. 1531-1545. London: Academic Press.

Baranova, A., Ivanov, D., Petrash, N., Pestova, A., Skoblov, M., Kelmanson, I., Shagin, D., Nazarenko, S., Geraymovych, E., Litvin, O. et al. (2004). The mammalian pannexin family is homologous to the invertebrate innexin gap junction family. *Genomics* **83**, 706-716.

Bauer, R., Lehmann, C., Martini, J., Eckardt, F. and Hoch, M. (2004). Gap junction channel protein innexin 2 is essential for epithelial morphogenesis in the Drosophila embryo. *Mol. Biol. Cell* **15**, 2992-3004.

Bauer, R., Löer, B., Ostrowski, K., Martini, J., Weimbs, A., Lechner, H. and Hoch, M. (2005). Intercellular communication: the Drosophila innexin multiprotein family of gap junction proteins. *Chem. Biol.* **12**, 515-526.

Bedner, P., Steinhäuser, C. and Theis, M. (2012). Functional redundancy and compensation among members of gap junction protein families? *Biochim. Biophys. Acta* **1818**, 1971-1984.

Benton, M. A., Akam, M. and Pavlopoulos, A. (2013). Cell and tissue dynamics during Tribolium embryogenesis revealed by versatile fluorescence labeling approaches. *Development* **140**, 3210-3220.

Bhalla-Gehi, R., Penuela, S., Churko, J. M., Shao, Q. and Laird, D. W. (2010). Pannexin1 and pannexin3 delivery, cell surface dynamics, and cytoskeletal interactions. *J. Biol. Chem.* **285**, 9147-9160.

Bucher, G., Scholten, J. and Klingler, M. (2002). Parental RNAi in Tribolium (Coleoptera). *Curr. Biol.* **12**, R85-R86.

Bullock, S. L., Stauber, M., Prell, A., Hughes, J. R., Ish-Horowicz, D. and Schmidt-Ott, U. (2004). Differential cytoplasmic mRNA localisation adjusts pair-rule transcription factor activity to cytoarchitecture in dipteran evolution. *Development* **131**, 4251-4261.

Crespin, S., Bechberger, J., Mesnil, M., Naus, C. C. and Sin, W.-C. (2010). The carboxy-terminal tail of connexin43 gap junction protein is sufficient to mediate cytoskeleton changes in human glioma cells. *J. Cell. Biochem.* **110**, 589-597.

D'hondt, C., Ponsaerts, R., De Smedt, H., Bultynck, G. and Himpens, B. (2009). Pannexins, distant relatives of the connexin family with specific cellular functions? *Bioessays* **31**, 953-974.

Ede, D. A. (1964). An Inherited abnormality affecting the development of the yolk plasmodium and endoderm in Dermestes Maculatus (Coleoptera). *J. Embryol. Exp. Morphol.* **12**, 551-562.

Fushiki, D., Hamada, Y., Yoshimura, R. and Endo, Y. (2010). Phylogenetic and bioinformatic analysis of gap junction-related proteins, innexins, pannexins and connexins. *Biomed. Res.* **31**, 133-142.

Galtier, N., Gouy, M. and Gautier, C. (1996). SEAVIEW and PHYLO_WIN: two graphic tools for sequence alignment and molecular phylogeny. *Comput. Appl. Biosci.* **12**, 543-548.

Giuliani, F., Giuliani, G., Bauer, R. and Rabouille, C. (2013). Innexin 3, a new gene required for dorsal closure in Drosophila embryo. *PLoS ONE* **8**, e69212.

Goodenough, D. A. and Paul, D. L. (2009). Gap junctions. *Cold Spring Harb. Perspect. Biol.* **1**, a002576.

Guindon, S. and Gascuel, O. (2003). A simple, fast, and accurate algorithm to estimate large phylogenies by maximum likelihood. *Syst. Biol.* **52**, 696-704.

Handel, K., Grünfelder, C. G., Roth, S. and Sander, K. (2000). Tribolium embryogenesis: a SEM study of cell shapes and movements from blastoderm to serosal closure. *Dev. Genes Evol.* **210**, 167-179.

Handel, K., Basal, A., Fan, X. and Roth, S. (2005). Tribolium castaneum twist: gastrulation and mesoderm formation in a short-germ beetle. *Dev. Genes Evol.* **215**, 13-31.

Harris, T. J. C., Sawyer, J. K. and Peifer, M. (2009). How the cytoskeleton helps build the embryonic body plan: models of morphogenesis from Drosophila. *Curr. Top. Dev. Biol.* **89**, 55-85.

Kumar, S., Tamura, K. and Nei, M. (2004). MEGA3: integrated software for Molecular Evolutionary Genetics Analysis and sequence alignment. *Brief. Bioinform.* **5**, 150-163.

Lagrée, V., Brunschwig, K., Lopez, P., Gilula, N. B., Richard, G. and Falk, M. M. (2003). Specific amino-acid residues in the N-terminus and TM3 implicated in channel function and oligomerization compatibility of connexin43. *J. Cell Sci.* **116**, 3189-3201.

Lecuit, T. (2004). Junctions and vesicular trafficking during Drosophila cellularization. *J. Cell Sci.* **117**, 3427-3433.

Lecuit, T. and Wieschaus, E. (2000). Polarized insertion of new membrane from a cytoplasmic reservoir during cleavage of the Drosophila embryo. *J. Cell Biol.* **150**, 849-860.

Lord, J. C., Hartzer, K., Toutges, M. and Oppert, B. (2010). Evaluation of quantitative PCR reference genes for gene expression studies in Tribolium castaneum after fungal challenge. *J. Microbiol. Methods* **80**, 219-221.

Mavrakis, M., Rikhy, R. and Lippincott-Schwartz, J. (2009). Plasma membrane polarity and compartmentalization are established before cellularization in the fly embryo. *Dev. Cell* **16**, 93-104.

Mazumdar, A. and Mazumdar, M. (2002). How one becomes many: blastoderm cellularization in Drosophila melanogaster. *Bioessays* **24**, 1012-1022.

Meşe, G., Richard, G. and White, T. W. (2007). Gap junctions: basic structure and function. *J. Invest. Dermatol.* **127**, 2516-2524.

Ostrowski, K., Bauer, R. and Hoch, M. (2008). The Drosophila innexin7 gap junction protein is required for development of the embryonic nervous system. *Cell Commun. Adhes.* **15**, 155-167.

Panchina, Y., Kelmanson, I., Matz, M., Lukyanov, K., Usman, N. and Lukyanov, S. (2000). A ubiquitous family of putative gap junction molecules. *Curr. Biol.* **10**, R473-R474.

Panfilio, K. A., Oberhofer, G. and Roth, S. (2013). High plasticity in epithelial morphogenesis during insect dorsal closure. *Biol. Open* **2**, 1108-1118.

Pelissier, A., Chauvin, J.-P. and Lecuit, T. (2003). Trafficking through Rab11 endosomes is required for cellularization during Drosophila embryogenesis. *Curr. Biol.* **13**, 1848-1857.

Phelan, P. (2005). Innexins: members of an evolutionarily conserved family of gap-junction proteins. *Biochim. Biophys. Acta* **1711**, 225-245.

Phelan, P. and Starich, T. A. (2001). Innexins get into the gap. *Bioessays* **23**, 388-396.

Riedl, J., Crevenna, A. H., Kessenbrock, K., Yu, J. H., Neukirchen, D., Bista, M., Bradke, F., Jenne, D., Holak, T. A., Werb, Z. et al. (2008). Lifeact: a versatile marker to visualize F-actin. *Nat. Methods* **5**, 605-607.

Riggs, B., Rothwell, W., Mische, S., Hickson, G. R. X., Matheson, J., Hays, T. S., Gould, G. W. and Sullivan, W. (2003). Actin cytoskeleton remodeling during early Drosophila furrow formation requires recycling endosomal components Nuclear-fallout and Rab11. *J. Cell Biol.* **163**, 143-154.

Rothwell, W. F., Fogarty, P., Field, C. M. and Sullivan, W. (1998). Nuclear-fallout, a Drosophila protein that cycles from the cytoplasm to the centrosomes, regulates cortical microfilament organization. *Development* **125**, 1295-1303.

Sarrazin, A. F., Peel, A. D. and Averof, M. (2012). A segmentation clock with two-segment periodicity in insects. *Science* **336**, 338-341.

Scemes, E. (2012). Nature of plasmalemmal functional "hemichannels". *Biochim. Biophys. Acta* **1818**, 1880-1883.

Scemes, E., Suadicani, S. O., Dahl, G. and Spray, D. C. (2007). Connexin and pannexin mediated cell–cell communication. *Neuron Glia Biol.* **3**, 199-208.

Scemes, E., Spray, D. C. and Meda, P. (2009). Connexins, pannexins, innexins: novel roles of "hemi-channels". *Pflugers Arch. Eur. J. Physiol.* **457**, 1207-1226.

Schejter, E. D. and Wieschaus, E. (1993). Functional elements of the cytoskeleton in the early drosophila embryo. *Annu. Rev. Cell Biol.* **9**, 67-99.

Schröder, R., Beermann, A., Wittkopp, N. and Lutz, R. (2008). From development to biodiversity—Tribolium castaneum, an insect model organism for short germband development. *Dev. Genes Evol.* **218**, 119-126.

Shestopalov, V. I. and Panchin, Y. (2008). Pannexins and gap junction protein diversity. *Cell. Mol. Life Sci.* **65**, 376-394.

Sokac, A. M. and Wieschaus, E. (2008a). Local actin-dependent endocytosis is zygotically controlled to initiate Drosophila cellularization. *Dev. Cell* **14**, 775-786.

Sokac, A. M. and Wieschaus, E. (2008b). Zygotically controlled F-actin establishes cortical compartments to stabilize furrows during Drosophila cellularization. *J. Cell Sci.* **121**, 1815-1824.

Sosinsky, G. E., Boassa, D., Dermietzel, R., Duffy, H. S., Laird, D. W., MacVicar, B., Naus, C. C., Penuela, S., Scemes, E., Spray, D. C. et al. (2011). Pannexin channels are not gap junction hemichannels. *Channels (Austin)* **5**, 193-197.

Wall, M. E., Otey, C., Qi, J. and Banes, A. J. (2007). Connexin 43 is localized with actin in tenocytes. *Cell Motil. Cytoskeleton* **64**, 121-130.

Warn, R. M. and Magrath, R. (1983). F-actin distribution during the cellularization of the *Drosophila* embryo visualized with FL-phalloidin. *Exp. Cell Res.* **143**, 103-114.

Zhang, C. X., Lee, M. P., Chen, A. D., Brown, S. D. and Hsieh, T. (1996). Isolation and characterization of a Drosophila gene essential for early embryonic development and formation of cortical cleavage furrows. *J. Cell Biol.* **134**, 923-934.